A&A 554, A54 (2013)
DOI: 10.1051/0004-6361/201321395

Astronomy & Astrophysics

A progenitor binary and an ejected mass donor remnant of faint type Ia supernovae

S. Geier[1,2], T. R. Marsh[3], B. Wang[4], B. Dunlap[5], B. N. Barlow[6], V. Schaffenroth[2,7], X. Chen[4], A. Irrgang[2], P. F. L. Maxted[8], E. Ziegerer[2], T. Kupfer[9], B. Miszalski[10,11], U. Heber[2], Z. Han[4], A. Shporer[12,13,14], J. H. Telting[15], B. T. Gänsicke[3], R. H. Østensen[16], S. J. O'Toole[17], and R. Napiwotzki[18]

[1] European Southern Observatory, Karl-Schwarzschild-Str. 2, 85748 Garching, Germany
e-mail: sgeier@eso.org
[2] Dr. Karl Remeis-Observatory & ECAP, Astronomical Institute, Friedrich-Alexander University Erlangen-Nürnberg, Sternwartstr. 7, 96049 Bamberg, Germany
[3] Department of Physics, University of Warwick, Conventry CV4 7AL, UK
[4] Key Laboratory of the Structure and Evolution of Celestial Objects, Yunnan Observatory, Chinese Academy of Sciences, 650011 Kunming, PR China
[5] Department of Physics and Astronomy, University of North Carolina, Chapel Hill, NC 27599-3255, USA
[6] The Pennsylvania State University, 525 Davey Lab, University Park, PA 16802, USA
[7] Institute for Astro- and Particle Physics, University of Innsbruck, Technikerstr. 25/8, 6020 Innsbruck, Austria
[8] Astrophysics Group, Keele University, Staffordshire, ST5 5BG, UK
[9] Department of Astrophysics/IMAPP, Radboud University Nijmegen, PO Box 9010, 6500 GL Nijmegen, The Netherlands
[10] South African Astronomical Observatory, PO Box 9, Observatory, 7935 Cape Town, South Africa
[11] Southern African Large Telescope Foundation, PO Box 9, Observatory, 7935 Cape Town, South Africa
[12] Las Cumbres Observatory Global Telescope Network, 6740 Cortona Drive, Suite 102, Santa Barbara, CA 93117, USA
[13] Department of Physics, Broida Hall, University of California, Santa Barbara, CA 93106, USA
[14] Division of Geological and Planetary Sciences, California Institute of Technology, Pasadena, CA 91125, USA
[15] Nordic Optical Telescope, Apartado 474, 38700 Santa Cruz de La Palma, Spain
[16] Institute of Astronomy, K.U. Leuven, Celestijnenlaan 200D, 3001 Heverlee, Belgium
[17] Australian Astronomical Observatory, PO Box 915, North Ryde NSW 1670, Australia
[18] Centre of Astrophysics Research, University of Hertfordshire, College Lane, Hatfield AL10 9AB, UK

Received 3 March 2013 / Accepted 16 April 2013

ABSTRACT

Type Ia supernovae (SN Ia) are the most important standard candles for measuring the expansion history of the universe. The thermonuclear explosion of a white dwarf can explain their observed properties, but neither the progenitor systems nor any stellar remnants have been conclusively identified. Underluminous SN Ia have been proposed to originate from a so-called double-detonation of a white dwarf. After a critical amount of helium is deposited on the surface through accretion from a close companion, the helium is ignited causing a detonation wave that triggers the explosion of the white dwarf itself. We have discovered both shallow transits and eclipses in the tight binary system CD-30°11223 composed of a carbon/oxygen white dwarf and a hot helium star, allowing us to determine its component masses and fundamental parameters. In the future the system will transfer mass from the helium star to the white dwarf. Modelling this process we find that the detonation in the accreted helium layer is sufficiently strong to trigger the explosion of the core. The helium star will then be ejected at such high velocity that it will escape the Galaxy. The predicted properties of this remnant are an excellent match to the so-called hypervelocity star US 708, a hot, helium-rich star moving at more than 750 km s^{-1}, sufficient for it to leave the Galaxy. The identification of both progenitor and remnant provides a consistent picture of the formation and evolution of underluminous SNIa.

Key words. binaries: spectroscopic – subdwarfs – supernovae: general

1. Introduction

The search for the progenitors of type Ia supernovae (SN Ia) is ongoing, but the observational evidence remains inconclusive. In the standard single-degenerate scenarios, mass is transferred in a stable way by either a main sequence star or a red giant to a white dwarf (WD) companion. In the double-degenerate scenario, a close binary consisting of two white dwarfs shrinks because of angular momentum lost by the emission of gravitational waves and eventually merges. Possible progenitor systems have been proposed for both channels, but not conclusively identified yet. Although most SN Ia form a homogeneous class, about one third of them differ significantly in their luminosities and other observational properties, and their proper classification is crucial when using such events as standard candles for cosmology (Wang & Han 2012).

It has been proposed that underluminous SN Ia originate from a so-called double-detonation of a white dwarf. After a critical amount of helium is deposited on the surface through accretion from a close companion, the helium is ignited causing a detonation wave that triggers the explosion of the white dwarf itself even if its mass is significantly lower than the Chandrasekhar

limit (Nomoto 1982; Woosley et al. 1986). Hydrodynamic simulations predict the explosion of a CO-WD with a minimum mass of only ~0.8 $M_\odot$ as underluminous SN Ia triggered by the ignition of an He-shell of ~0.1 $M_\odot$ (Fink et al. 2010) in this so-called double-detonation scenario. Helium stars have already been proposed as possible donors for the single-degenerate scenario (Yoon & Langer 2003; Wang et al. 2009a,b) conveniently explaining the lack of hydrogen in the spectra of SN Ia. Recent studies indicate that this scenario might also be consistent with the lack of helium in standard SN Ia spectra as long as the accreted He-layer is thin (Sim et al. 2010; Kromer et al. 2010).

In the course of the MUCHFUSS project (Geier et al. 2011), which aims at finding hot subdwarf binary systems with massive companions, we have discovered a possible progenitor for such a supernova consisting of a hot subdwarf B star (sdB) and a white dwarf in an extremely compact binary (Heber et al. 2013; Geier et al. 2013). This system, CD-30°11223, was also independently discovered by Vennes et al. (2012).

Hot subdwarf stars are evolved, core helium-burning objects. About half of the sdB stars reside in close binaries with periods ranging from ~0.1 d to ~30 d (Maxted et al. 2001; Napiwotzki et al. 2004a). The sdB is the core of a former red giant star that has been stripped of almost all of its hydrogen envelope through interaction with a companion star. The mass of the emerging sdB star is constrained to about half a solar mass in order to allow central helium burning. After the helium-burning phase the sdB star will turn into a white dwarf.

Because the separation of the components in these systems is much less than the size of the subdwarf progenitor in its red-giant phase, these systems must have experienced a common-envelope (CE) and spiral-in phase (Han et al. 2002, 2003 and references therein). In this scenario, a star evolving to become a red giant swallows a nearby companion. Because of friction, the core of the giant and the more compact companion spiral towards each other in a common envelope. The orbital energy lost during this process is deposited in the envelope until the envelope is eventually ejected leaving a close binary system as a remnant.

Although most of the close companions to sdB stars are low-mass main sequence stars, brown dwarfs, or low-mass WDs (~0.5 $M_\odot$), more massive compact companions like WDs, neutron stars, or black holes have been either observed or predicted by theory (Geier et al. 2007, 2010). The short-period sdB+WD binary KPD 1930+2752 is regarded as a progenitor candidate for an SN Ia (Maxted et al. 2000; Geier et al. 2007).

Here we report the discovery of both shallow transits and eclipses in the tight binary system CD-30°11223 composed of a carbon/oxygen white dwarf and a hot helium star, allowing us to determine its component masses and fundamental parameters. This system turns out to be an excellent progenitor candidate for the double-detonation SN Ia scenario and can be linked to the hypervelocity subdwarf US 708, the likely donor remnant of such an event.

2. Observations

The star CD-30°11223 (α_{2000} = $14^h11^m16\overset{s}{.}2$, δ_{2000} = −30°53′03″, m_V = 12.3 mag) was selected as a UV-excess object and spectroscopically identified to be an sdB star (Vennes et al. 2011; Németh et al. 2012). We selected this star as a bright backup target for our MUCHFUSS follow-up campaign. Because of unfavourable observing conditions, which prevented us from observing our main targets, two medium resolution spectra ($R \sim 2200, \lambda = 4450–5110$ Å) were taken consecutively with the EFOSC2 spectrograph mounted at the ESO NTT on June 10, 2012. The radial velocity shift between those two spectra turned out to be as high as 600 km s^{-1}.

The first spectroscopic follow-up data was obtained with the grating spectrograph mounted on the SAAO-1.9 m telescope on July 2, 2012. The RV-curve derived from 18 single spectra confirmed the short orbital period of 0.0498 d and a high RV-semiamplitude ($K = 370 \pm 14$ km s^{-1}). In order to improve the orbital solution and minimize the effect of orbital smearing, we took another 105 spectra with the ISIS spectrograph ($R \sim 4000, \lambda = 3440–5270$ Å, $T_{\rm exp} = 2$ min) mounted at the WHT during a dedicated MUCHFUSS follow-up run from July 9 to 12, 2012. Another 175 spectra were taken with the Goodman spectrograph mounted at the SOAR telescope ($R \sim 7700, \lambda = 3700–4400$ Å, $T_{\rm exp} = 1$ min) on July 16, 2012.

CD-30°11223 was observed by the SuperWASP planetary transit survey (Pollacco et al. 2006). The light curve contains 23 678 measurements taken from May 4, 2006 to August 1, 2011. On July 6, 2012, 3.6 h of time-series photometry in the V-band ($T_{\rm exp} = 3$ s) were taken with SOAR/Goodman under photometric conditions. The light curve was extracted using an aperture that minimizes the standard deviation of the two comparison stars used divided by each other at low airmass; a flat-field correction was also applied. The combination of short exposure times and bright stars makes scintillation the dominant noise source for our photometry. Another source of noise was likely caused by a small scatter in effective integration time of the order of a few ms.

3. Orbital and atmospheric parameters

The light curve shows variations caused by the ellipsoidal deformation of the sdB primary, which is triggered by the tidal influence of the compact companion. The light curve also shows Doppler boosting, caused by the extreme orbital motion of the sdB (Shakura & Postnov 1987; see also Bloemen et al. 2011, and references therein). The ephemeris has been derived from the SWASP data based on fitting a harmonic series. Because of the timebase of more than five years, the derived orbital period of 0.0489790724 ± 0.0000000018 d is very accurate and perfectly consistent with the independent determination (P = 0.04897906 ± 0.00000004 d) by Vennes et al. (2012).

The radial velocities were measured by fitting a set of mathematical functions to the hydrogen Balmer lines as well as helium lines using the FITSB2 routine (Napiwotzki et al. 2004b). Three functions (Gaussians, Lorentzians, and polynomials) are used to match the continuum, the line and the line core, respectively and mimic the typical Voigt profile of spectral lines. The profiles are fitted to all suitable lines simultaneously using χ^2-minimization, and the RV shift with respect to the rest wavelengths is measured. Assuming circular orbits, sine curves were fitted to the RV data points in fine steps over a range of test periods. The two datasets obtained with ISIS and Goodman are treated separately to investigate systematic errors. Details about the analysis method and error estimation are given in Geier et al. (2011). The derived orbital parameters from the ISIS dataset (K = 378.6 ± 1.0 km s^{-1}, γ = 17.6±0.7 km s^{-1}, see Fig. 1, lower panel) and the Goodman dataset (K = 374.5±1.1 km s^{-1}, γ = 21.3±0.8 km s^{-1}, see Fig. 1, upper panel) are consistent, taking into account that systematic uncertainties are usually somewhat higher than the statistical 1 σ errors given here. The deviation in system velocity is most likely caused by a slight systematic zero-point shift

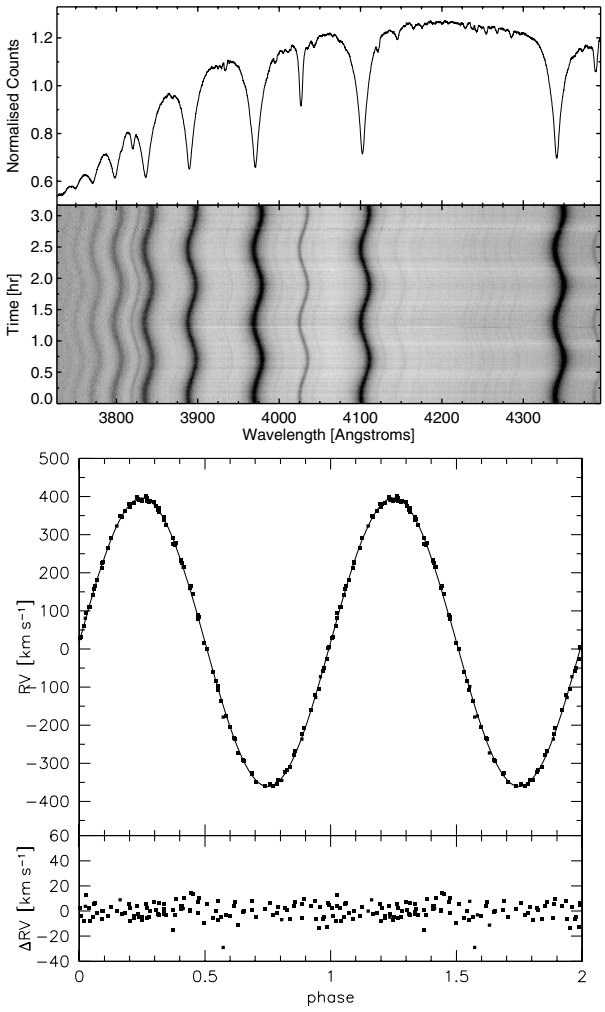

Fig. 1. *Upper panel*: spectrum of CD-30°11223 coadded from 175 RV-corrected spectra taken with SOAR/Goodman. The hydrogen Balmer series is clearly visible, as well as a prominent helium line at 4026 Å. The other features are rotationally broadened metal lines. Model spectra were matched to the hydrogen and helium lines to determine the atmospheric parameters of the hot subdwarf star. *Middle panel*: trailed spectra taken with SOAR/Goodman and showing the short-period sinusoidal variations of the Doppler-shifted spectral lines caused by the motion of the visible sdB star. The close and compact white-dwarf companion of the subdwarf star is not visible in this dataset. *Lower panel*: radial velocity curve of CD-30°11223 derived from 105 spectra taken with WHT/ISIS plotted twice against orbital phase for better visualisation.

between the two instruments. For further analysis we used the average values. Those values are in reasonable agreement with the results ($K = 386.9 \pm 1.9$ km s^{-1}, $\gamma = 31.5 \pm 1.3$ km s^{-1}) of Vennes et al. (2012), although somewhat discrepant.

The atmospheric parameters of effective temperature $T_{\rm eff}$, surface gravity $\log g$, helium abundance, and projected rotational velocity were determined by fitting simultaneously the observed hydrogen and helium lines of the single spectra with metal-line-blanketed LTE model spectra (Heber et al. 2000) as described in Geier et al. (2007). No significant variations of the parameters with orbital phase have been detected. Average values and standard deviations have been calculated separately for the ISIS dataset ($T_{\rm eff} = 28\,800 \pm 200$ K, $\log g = 5.67 \pm 0.03$, $\log y = -1.50 \pm 0.07$, $v_{\rm rot} \sin i = 180 \pm 8$ km s^{-1}, see Figs. 2, 3) and the Goodman dataset ($T_{\rm eff} = 29\,600 \pm 300$ K, $\log g = 5.65 \pm 0.05$, $\log y = -1.46 \pm 0.14$, $v_{\rm rot} \sin i = 174 \pm 12$ km s^{-1}). We adopt the average values from both datasets for further analysis. The final helium abundance is taken from the ISIS data because of the higher number of He-lines in the spectral range.

The derived parameters are consistent with literature values within the uncertainties (Vennes et al. 2011; Németh et al. 2012). More detailed information about the systematic errors of this method can be found in Geier et al. (2007, 2011). Table 1 shows the orbital and atmospheric parameters, Fig. 4 the position of CD-30°11223 in the $T_{\rm eff} - \log g$ diagram.

4. Light curve analysis

The light curve obtained with SOAR/Goodman was analysed by fitting models calculated with the LCURVE code written by TRM (see Fig. 5, Copperwheat et al. 2010). The code uses grids of points modelling the two stars and takes into account limb darkening, gravity darkening, mutual illumination effects, Doppler boosting, and gravitational lensing. Since the masses and radii of both components are strongly correlated, those parameters have been constrained using Markov chain Monte Carlo simulations. A detailed description of the analysis method is given by Bloemen et al. (2011).

In order to determine masses and radii of both the sdB and the WD, we used two different prior constraints. In each case the K derived from spectroscopy is used. First, we assumed tidal synchronisation of the sdB primary (solution 1), which is a reasonable assumption given the short orbital period of the system. The $v_{\rm rot} \sin i$ derived from spectroscopy is measured making the simplified assumption of a spherical, linear limb darkened star (limb darkening coefficient 0.3). To take into account the additional effects of limb darkening and gravitational darkening of the Roche-distorted star we calculated a correction factor of 0.963 by comparing the slightly different line profiles calculated under both assumptions (Claret & Bloemen 2011). This correction was applied to the $v_{\rm rot} \sin i$ before deriving the binary parameters. The best fit is achieved for an sdB mass of $0.47 \pm 0.03\ M_\odot$ and a WD mass of $0.74 \pm 0.02\ M_\odot$. However, we found that the radius of the WD is about 10% smaller than predicted by the zero-temperature mass-radius relation for WDs, which provides a lower limit for the WD radius (see Fig. 6, second panel from top, Verbunt & Rappaport 1988).

To explore the influence of this discrepancy, we imposed the restriction that the white dwarf should be within 2% of the M-R-relation and allowed for deviations from corotation (solution 2). We determined an estimate for the temperature of the WD from our light curve analysis. Since we see a significant feature when the sdB occults the WD, we can derive a black-body temperature of $24\,700 \pm 1200$ K for the WD, which leads to a radius about 5% higher than expected from the zero-temperature relation. We adopt this more realistic value for our analysis. In this case the derived masses are somewhat higher ($M_{\rm sdB} = 0.54 \pm 0.02\ M_\odot$, $M_{\rm WD} = 0.79 \pm 0.01\ M_\odot$).

Although both solutions are consistent within their uncertainties, we refrain from favouring one over the other. To calculate the kinematics and the further evolution of the system, we adopt the average values for the component masses ($M_{\rm sdB} = 0.51\ M_\odot$, $M_{\rm WD} = 0.76\ M_\odot$, see Fig. 6).

Comparing the derived sdB masses with evolutionary tracks for core helium-burning objects (Fig. 4), it can be seen that the appropriate tracks are consistent with the position of CD-30°11223 in the $T_{\rm eff} - \log g$ diagram. Furthermore, the effective temperature and surface gravity of the star tell us that the

Table 1. Parameters of the CD-30°11223 system.

Visual magnitude[†]	m_V	[mag]	12.342 ± 0.003
Proper motion[‡]	$\mu_\alpha \cos\delta$	[mas/yr]	9.5 ± 2.2
	μ_δ	[mas/yr]	−5.6 ± 2.2
Atmospheric parameters of the subdwarf			
Effective temperature	$T_{\rm eff}$	[K]	29 200 ± 400
Surface gravity	$\log g$		5.66 ± 0.05
Helium abundance	$\log y$		−1.50 ± 0.07
Projected rotational velocity	$v_{\rm rot} \sin i$	[km s^{-1}]	177 ± 10
Orbital parameters			
	T_0	[BJD UTC]	2 455 113.205908 ± 0.000363
Orbital period	P	[d]	0.0489790724 ± 0.0000000018
RV semi-amplitude	K	[km s^{-1}]	376.6 ± 1.0
System velocity	γ	[km s^{-1}]	19.5 ± 2.0
Binary mass function	$f(M)$	[$M_\odot$]	0.271 ± 0.002
Derived parameters			
Solution 1			
sdB mass	$M_{\rm sdB}$	[$M_\odot$]	0.47 ± 0.03
sdB radius	$R_{\rm sdB}$	[$R_\odot$]	0.169 ± 0.005
WD mass	$M_{\rm WD}$	[$M_\odot$]	0.74 ± 0.02
WD radius	$R_{\rm WD}$	[$R_\odot$]	0.0100 ± 0.0004
Orbital inclination	i	[°]	83.8 ± 0.6
Separation	a	[$R_\odot$]	0.599 ± 0.009
Mass ratio	q		0.63 ± 0.02
Solution 2			
sdB mass	$M_{\rm sdB}$	[$M_\odot$]	0.54 ± 0.02
sdB radius	$R_{\rm sdB}$	[$R_\odot$]	0.179 ± 0.003
WD mass	$M_{\rm WD}$	[$M_\odot$]	0.79 ± 0.01
WD radius	$R_{\rm WD}$	[$R_\odot$]	0.0106 ± 0.0002
Orbital inclination	i	[°]	82.9 ± 0.4
Separation	a	[$R_\odot$]	0.619 ± 0.005
Mass ratio	q		0.68 ± 0.01

Notes. [(†)] The visual magnitude is taken from Vennes et al. (2012). [(‡)] Proper motions taken from Roeser et al. (2010).

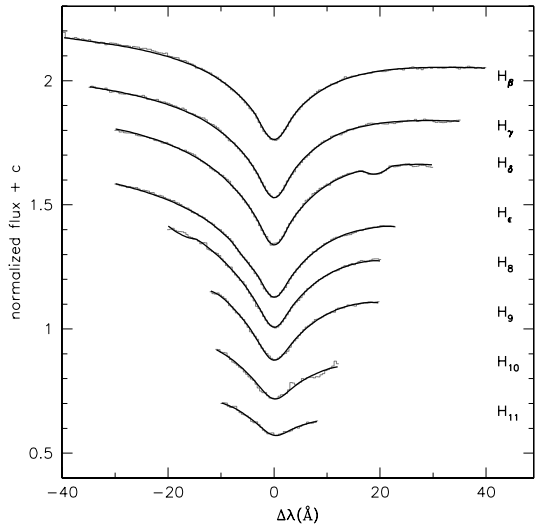

Fig. 2. Fit of synthetic LTE models to the hydrogen Balmer lines of a coadded ISIS spectrum. The normalized fluxes of the single lines are shifted for better visualisation.

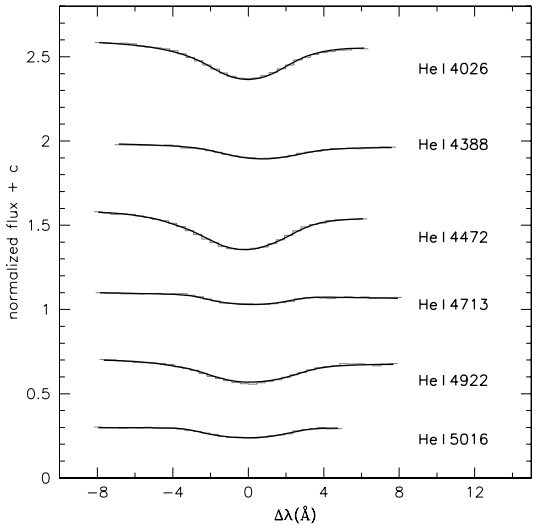

Fig. 3. Fit of synthetic LTE models to the helium lines (see Fig. 2).

sdB has just recently been formed and started the core helium-burning phase, which typically lasts for about 100 Myr.

5. Gravitational wave radiation

Because of its short orbital period, CD-30°11223 is expected to be a strong source of gravitational waves. We therefore calculated the current gravitational wave emission of CD-30°11223. The gravitational wave strain amplitude h scales with the masses of both binary components, the binary inclination, the orbital period and the distance of the system.

We calculate it as described in Roelofs et al. (2007) to be as high as $\log h = -21.5 \pm 0.3$; CD-30°11223 should therefore be one of the strongest gravitational wave sources detectable with missions like NGO/eLISA (Kilic et al. 2012; Nelemans 2009).

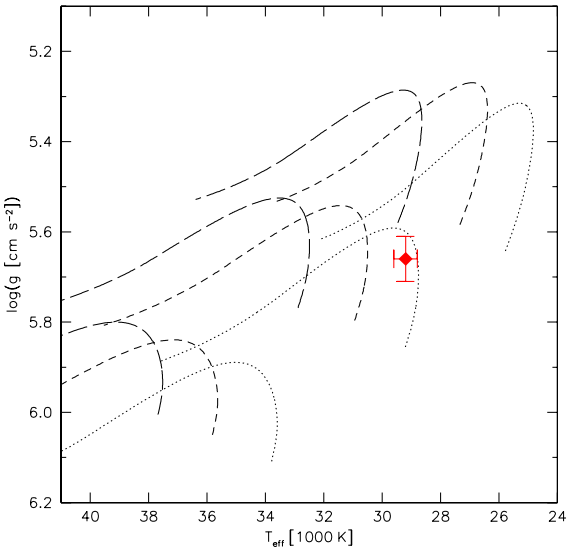

Fig. 4. $T_{\rm eff} - \log g$ diagram. Evolutionary tracks (solar metallicity) of core helium-burning stars with masses of 0.45 $M_\odot$ (dotted lines), 0.50 $M_\odot$ (short-dashed lines) and 0.55 $M_\odot$ (long-dashed lines) are plotted for different hydrogen envelope masses (0.000 $M_\odot$, 0.001 $M_\odot$, 0.005 $M_\odot$, from the lower left to the upper right). The diamond marks CD-30°11223.

It is even more noticeable, because the presence of eclipses allows us determine its binary parameters to very high accuracy. Therefore, this system can be used as a verification source for upcoming space missions.

No period change due to the orbital shrinkage caused by the emission of gravitational wave radiation has been detected in the SWASP data ($\dot{P} = 1.01 \times 10^{-12} \pm 3.38 \times 10^{-12}$ s s^{-1}). This non-detection is consistent with the theoretically expected value of $\dot{P} \sim 6 \times 10^{-13}$ s s^{-1}. However, within only a few more years the orbital shrinkage should become detectable.

6. Binary evolution calculations

More interesting than the present state of this system is its future evolution, which can now be studied in detail using theoretical models. Employing Eggleton's stellar evolution code (Eggleton 1971, 1972, 1973), we calculated the evolution of the sdB star and its WD companion. The code has been updated with the latest input physics over the past four decades (Han et al. 1994; Pols et al. 1995, 1998). Roche lobe overflow (RLOF) is treated within the code described by Han et al. (2000). We set the ratio of mixing length to local pressure scale height, $\alpha = l/H_{\rm p}$, to be 2.0. We assume that the binary model starts with a 0.51 $M_\odot$ He star and a 0.76 $M_\odot$ CO WD having a 0.049 d orbit period, similar to the initial model of the sdB star and its WD companion. Additionally, orbital angular momentum loss due to gravitational wave radiation is included by adopting a standard formula presented by Landau & Lifshitz (1971)

$$\frac{{\rm d}\ln J_{\rm GR}}{{\rm d}t} = -\frac{32G^3}{5c^5}\,\frac{M_{\rm WD}M_2(M_{\rm WD}+M_2)}{a^4}, \qquad (1)$$

where G, c, $M_{\rm WD}$, and M_2 are the gravitational constant, vacuum speed of light, the mass of the accreting WD, and the mass of the companion sdB star, respectively.

In the He double-detonation model, if the mass-accretion rate is higher than 4×10^{-8} $M_\odot$ yr^{-1}, the WD can increase its mass (Woosley et al. 1986; Wang et al. 2009a). However, for low mass-accretion rates (1×10^{-9} $M_\odot$ yr^{-1} $\lesssim |\dot{M}_2| \lesssim 4 \times 10^{-8}$ $M_\odot$ yr^{-1}), compressional heating at the base of the accreted He layer plays no significant role, and a layer of unburned He can be accumulated on the surface of the WD. If the mass-accretion rate is slower ($|\dot{M}_2| < 1 \times 10^{-9}$ $M_\odot$ yr^{-1}), the He flash is strong enough to form a He detonation, but too weak to initiate a carbon detonation, and only a single He detonation wave propagates outward (Nomoto 1982).

We assume that if a CO WD accumulating He enters this "low" accretion rate regime and accumulates 0.1 $M_\odot$ of He on its surface, a detonation is initiated at the base of the He shell layer (Fink et al. 2010). Consequently, a detonation in the core of the CO WD is presumed to follow, in which a sub-$M_{\rm Ch}$ SN Ia takes place. In this model, only accreting WDs with a total mass (CO core 0.8 $M_\odot$ + helium shell 0.1 $M_\odot$) $\geq$ 0.9 $M_\odot$ are considered to result in potential sub-$M_{\rm Ch}$ SNe Ia, since the CO-core with lower mass may not detonate and it is unlikely to produce enough radioactive nickel observed in SNe Ia (Kromer et al. 2010).

The binary system starts with ($M_2^{\rm i}$, $M_{\rm WD}^{\rm i}$, $\log(P^{\rm i}/{\rm d})$) = (0.510, 0.760, −1.310), where $M_2^{\rm i}$ and $M_{\rm WD}^{\rm i}$ are the initial masses of the He star star and of the CO WD in solar mass, and $P^{\rm i}$ is the initial orbital period in days. Figure 7 (left panel) shows the evolutionary track of the He star and the evolution of the orbital period. The right panel displays the mass-transfer rate and the mass of the WD envelope varying with time after the He star fills its Roche lobe.

Because of the short initial orbital period (0.049 d) of the system, angular momentum loss induced by gravitational wave radiation is large. This leads to the rapid shrinking of the orbital separation. After about 36 million years, the He star begins to fill its Roche lobe while it is still in the core helium-burning stage. The mass-transfer rate is stable and at a low rate between 1.6×10^{-8} $M_\odot$ yr^{-1} and 2.2×10^{-8} $M_\odot$ yr^{-1}, resulting in the formation of a He shell on the surface of the CO WD. After about 6 million years, the mass of the He shell increases to ∼0.1 $M_\odot$ in which a double-detonation may happen at the base of the He shell layer. At this moment, the mass of the He star is $M_2^{\rm SN} = 0.41$ $M_\odot$ and the orbital period is $\log(P^{\rm SN}/{\rm d}) = -1.72$ ($P = 0.019$ d).

7. Hypervelocity sdO as donor remnant

Theoretical predictions about whether or not a progenitor candidate will explode as a SN Ia are useful, but in general difficult to test. Usually the theoretically predicted SN rates are compared to the observed rates, but these comparisons are often hampered by selection effects. A more direct proof would be the identification of the remnant objects. We therefore follow the future evolution of CD-30°11223. At the end of the He-accretion phase and just before the SN event, the orbital period of the binary is predicted to have shrunk to 0.019 d as a result of the further loss of orbital energy through the emission of gravitational waves. The sdB primary lost a fair amount of mass (∼0.1 $M_\odot$), which was transferred to the WD companion. The orbital velocity of the sdB will be about 600 km s^{-1} and therefore close to the Galactic escape velocity. As soon as the WD is disrupted, the sdB will be ejected. Depending on the ejection direction of such an object relative to its trajectory around the Galactic centre, the Galactic rest frame velocity could be even higher by up to 240 km s^{-1}. In this case the remnant star will leave the Galaxy.

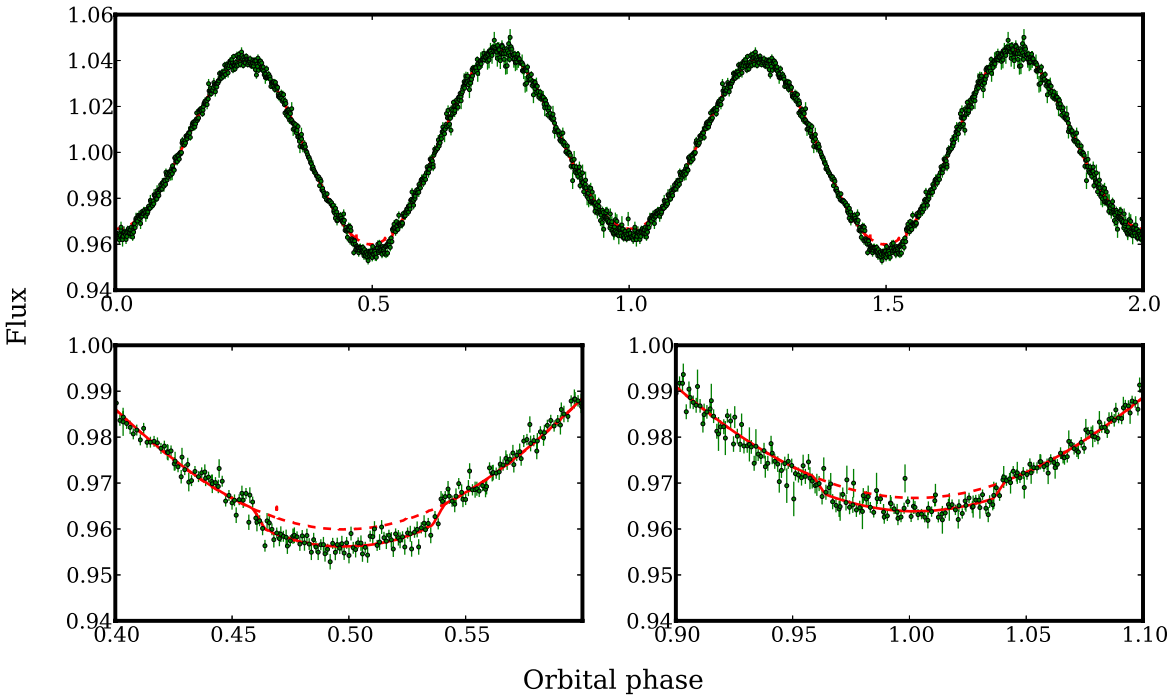

Fig. 5. *Upper panel*: V-band light curve of CD-30°11223 taken with SOAR/Goodman (green) with superimposed model (red) plotted twice against the orbital phase for better visualisation. The dashed red curve marks the same model without transits and eclipses. The sinusoidal variation is caused by the ellipsoidal deformation of the hot subdwarf as a result of the tidal influence of the compact white dwarf. The difference in the maxima between phase 0.25 and 0.75 originates from the relativistic Doppler boosting effect, which is usually not detectable with ground-based telescopes. *Lower panels*: close-up on the transit of the WD in front of the sdB (*left*). It is even possible to detect the eclipse of the WD by the sdB (*right*).

Such so-called hypervelocity stars have indeed been discovered (Brown et al. 2005; Hirsch et al. 2005; Edelmann et al. 2005). However, all but one of the known 22 objects are intermediate-mass main-sequence star. This enigmatic star (US 708) has been classified as a helium-rich hot subdwarf travelling at a Galactic rest frame velocity of at least 750 km s^{-1} (Hirsch et al. 2005), which matches the predicted ejection velocity of CD-30°11223 very well. It was proposed that this star might be the ejected He-donor after the WD companion exploded as a SN Ia (Justham et al. 2009; Wang & Han 2009).

In this scenario, the compact binary CD-30°11223 and the hypervelocity star US 708 represent two different stages of an evolutionary sequence linked by a SN Ia explosion. The existence of objects like US 708 thus provides evidence that binaries like CD-30°11223 are viable SN Ia progenitor candidates.

8. Age of the binary system

The analysis of our data also allows us to constrain the initial component masses and the age of the binary. Furthermore, we can constrain both its past and future trajectory.

8.1. Kinematic analysis

Using a standard Galactic gravitational potential with a Sun-Galactic centre distance of 8.4 kpc and a local standard of rest circular motion of 242 km s^{-1} (see Model I in Irrgang et al. 2013), we computed the past and future trajectory of CD-30°11223 (see Fig. 8). The orbit shows the typical characteristics of the local thin disc population, i.e. almost circular motion around the Galactic centre and small oscillations in direction perpendicular to the Galactic disc. The heliocentric distance to the star increases during the next 42 Myr until the supernova is predicted to explode from its current value of 364 ± 31 pc to about 1920 ± 160 pc.

The binary CD-30°11223 is by far the closest known SN Ia progenitor with respect to the Earth. The explosion will take place in a direction of the sky close to the current positions of the constellations Ara and Norma. Adopting an absolute visual magnitude of up to −19 mag for the SN Ia, the apparent magnitude seen from the Earth might be as high as ∼−7.6 mag or about as bright as SN 1006, the brightest stellar event in recorded history so far (Winkler et al. 2003).

8.2. Binary formation scenario

The system CD-30°11223 is the closest sdB binary known so far and the mass of its WD companion is higher than the average mass of CO WDs (∼0.6 $M_\odot$). To explore the formation of this exceptional system, we performed a binary population synthesis study in a similar way to the method described by Han et al. (2002, 2003). For given WD masses ranging from 0.6 $M_\odot$ to 1.4 $M_\odot$, an initial set of 10^6 WD+MS binaries was generated. For the main sequence stars the initial mass function of Salpeter was used. The orbital period distribution was assumed to be flat in $\log a$. The binaries were evolved through the common envelope phase for different values of the CE-efficiency parameters $\alpha_{\rm CE}$, which is the fraction of the available orbital energy used to eject the envelope, and $\alpha_{\rm th}$, the contributed fraction of internal energy.

In the standard scenario, which is called the 2nd CE channel, the progenitor of the sdB is a main sequence star of about solar mass and the common envelope is ejected right at the tip of the first giant branch (FGB, Han et al. 2002). However, this channel is not appropriate to form binaries as close as CD-30°11223, as

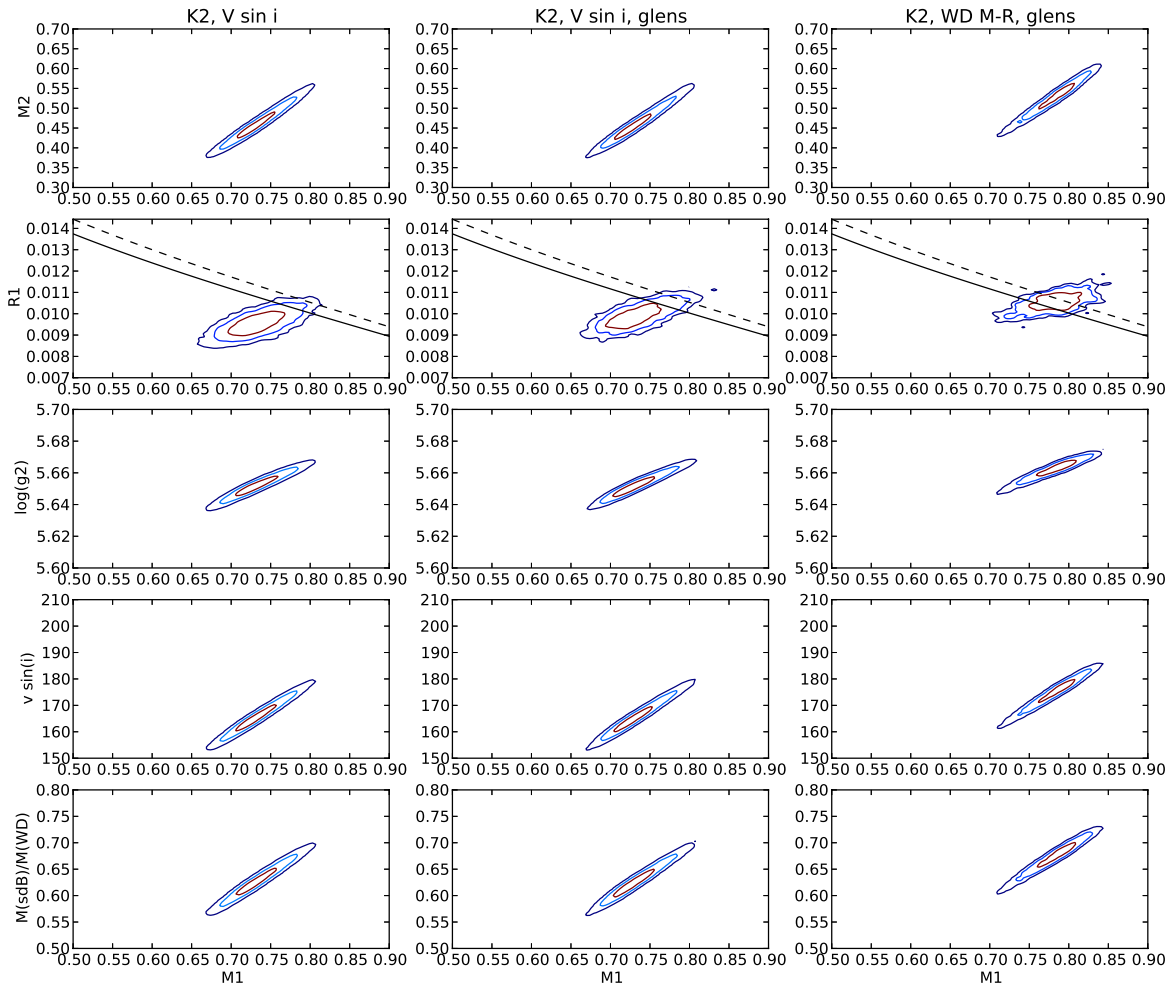

Fig. 6. Parameters of the CD-30°11223 system plotted against the mass of the WD companion with contours marking the 1σ (red), 2σ (light blue), and 3σ (dark blue) levels of confidence. In the *left column* tidal synchronisation of the sdB primary is assumed, while in the *middle column* the effect of microlensing has also been taken into account. Instead, in the *right column* the WD mass-radius relation has been used as an additional constraint. The solid lines in the mass-radius plots (*second panels from the top*) mark the zero-temperature mass-radius relation for WDs, the dashed lines more realistic models with 5% inflation. Note that both the $v_{\rm rot} \sin i$ and the $\log g$ derived from the light curve are in agreement with the values derived from spectroscopy.

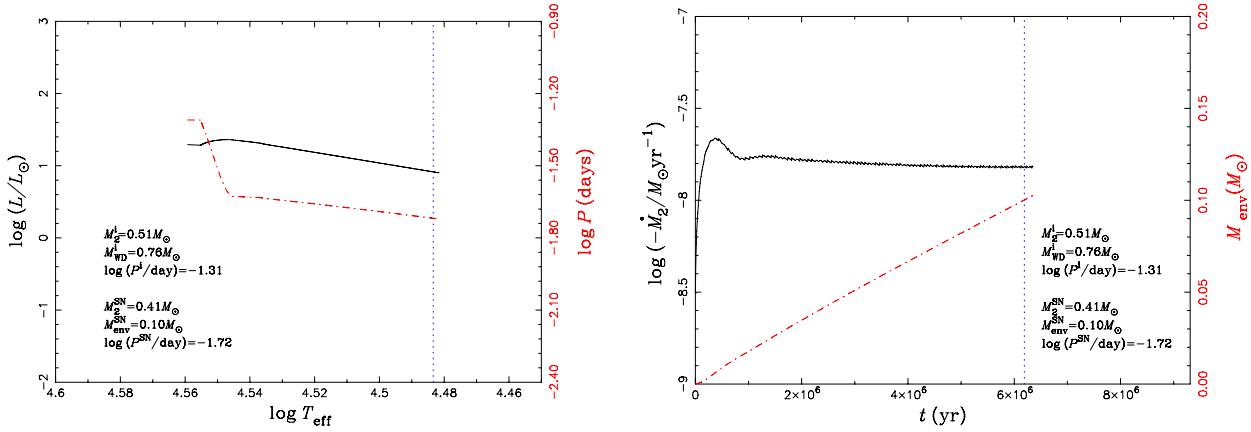

Fig. 7. Results of binary evolution calculations with initial masses of the two components and the orbital period similar to the sdB+WD binary system. *Left panel*: the evolutionary track of the He star is shown as a solid curve and the evolution of the orbital period as a dash-dotted curve. *Right panel*: the solid and dash-dotted curves show the mass-transfer rate and the mass of the WD envelope (He shell) varying with time after the He star fills its Roche lobe, respectively. Dotted vertical lines in both panels indicate the position where the double-detonation may happen (the mass of the He shell increases to ~0.1 $M_\odot$). The initial binary parameters and the parameters at the moment of the SN explosion are also given in the two panels.

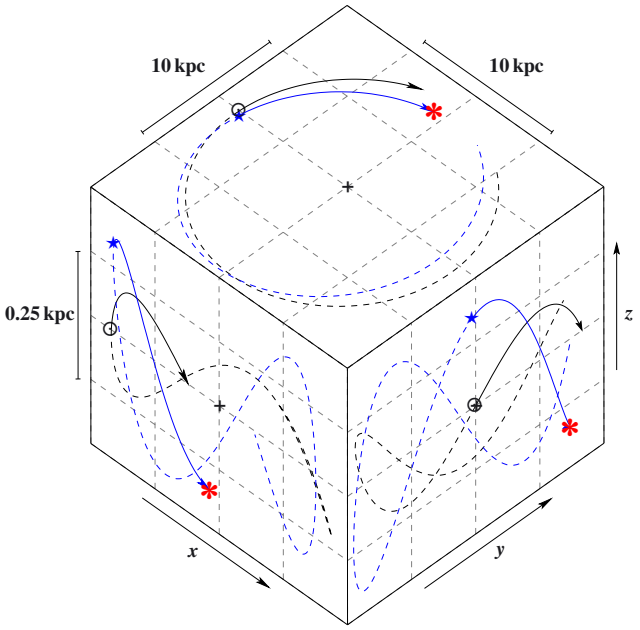

Fig. 8. Three-dimensional trajectory of CD-30°11223 in a Cartesian Galactic coordinate system with the z-axis pointing to the north Galactic pole. Current positions of CD-30°11223 (blue ⋆), Sun (black ⊙), and Galactic centre (black +) are marked. The approximate point in time of the supernova explosion is symbolized by the red asterisk, while the arrow marks the position of the Sun at that time. Solid lines indicate the future 42 Myr, dashed lines the past 150 Myr. CD-30°11223's kinematic properties are obviously those of the local thin disc population.

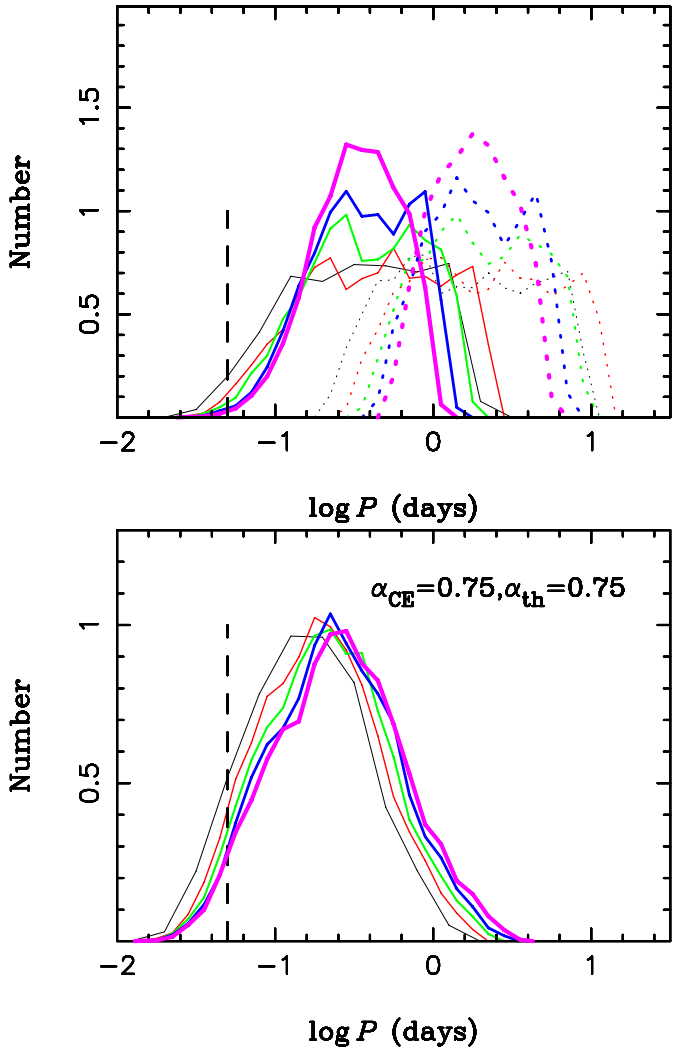

Fig. 9. *Top panel*: orbital period distribution of sdB+WD binaries from the 2nd CE channel. Different colours mark different WD masses (black 0.6 $M_\odot$, red 0.8 $M_\odot$, green 1.0 $M_\odot$, blue 1.2 $M_\odot$, purple 1.4 $M_\odot$). The vertical dashed line marks P = 0.05 d. The contribution of thermal energy has not been included (α_{th} = 0). The solid lines are for α_{CE} = 0.3 and the dotted ones for α_{CE} = 1.0. *Bottom panel*: orbital period distribution of sdB+WD binaries from the CE channel involving more massive main sequence stars (i.e. >2 $M_\odot$). The values of α_{CE} and α_{th} are indicated in the figure (see Fig. 9).

shown in Fig. 9 (upper panel). The envelope at the tip of the FGB has a very low binding energy and can be ejected easily in the following CE. Thus, the orbital shrinkage during CE evolution is not significant and the produced sdB+WD system generally has an orbital period much longer than that of CD-30°11223. Only for a very small value of α_{CE} = 0.3, which is very unlikely, some binaries reach the margin of 0.05 d. Indeed, the median period of the observed sdB binaries is as high as ~0.6 d (Geier et al. 2011). However, an sdB+WD binary can also be formed when the main-sequence progenitor of the subdwarf has an initial mass larger than 2 $M_\odot$ and fills its Roche lobe during the Hertzsprung Gap or at the base of the FGB. In this case, the envelope is more tightly bound and the orbital shrinkage required to eject the CE becomes higher. In Fig. 9 (lower panel) the orbital period distribution is shown for this scenario when $\alpha_{CE} = \alpha_{th} = 0.75$, similar to the best fitting model of Han et al. (2003). As seen in the figure, short orbital periods, just as in the case of CD-30°11223, are expected.

We also investigated the distribution of sdB masses formed via this channel. While the standard CE-scenario predicts a mass distribution with a sharp peak at 0.47 $M_\odot$, the sdB masses from more massive main-sequence stars (i.e. >2 $M_\odot$) show a significant scatter for higher values of α_{CE}, and even more so if we allow for a contribution of thermal energy in the CE-process by increasing the parameter α_{th}. The sdB mass for this channel largely depends on the mass of the progenitor, and can range from 0.3 to 1.0 $M_\odot$ (see Fig. 10). This is consistent with the sdB mass of up to 0.54 $M_\odot$ determined in the case of CD-30°11223.

We therefore conclude that CD-30°11223 was most likely formed via CE-ejection of a main sequence star with a mass larger than 2 $M_\odot$, which means that it originated from a young stellar population.

8.3. White dwarf cooling age and progenitor masses

We derived a mass of 0.76 $M_\odot$ for the WD companion based on observations. Using an initial-to-final mass relation for isolated WDs the mass of the progenitor should have ranged from 3 to 4 $M_\odot$ (see Fig. 7 in Kovetz et al. 2009, and references therein). Binary evolution is expected to lower the mass of the final WD and this progenitor mass estimate, therefore, has to be considered as lower limit.

Assuming a lifetime on the main sequence $\tau_{MS} = 10^{10}\,\mathrm{yr} \times [M/M_\odot]^{-2.5}$, the progenitor lived for a maximum of 640 Myr. We constrain the temperature of the WD in our light curve analysis to be ~25 000 K. Therefore, its cooling age is ~30–40 Myr[1].

[1] Taken from cooling models for mixed C/O composition and for standard thick H and He layers, http://www.astro.umontreal.ca/~bergeron/CoolingModels/, Fontaine et al. (2001).

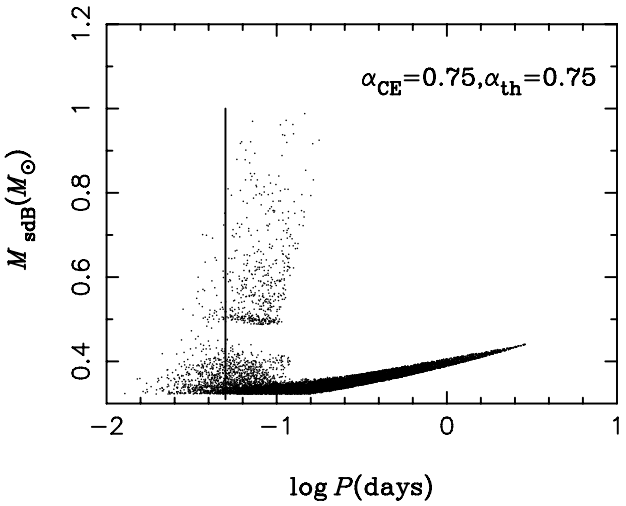

Fig. 10. sdB mass is plotted over the orbital period assuming the mass of the WD to be 1.2 $M_\odot$. The main-sequence progenitors of the sdBs have initial masses larger than 2 $M_\odot$. The values of α_{CE} and α_{th} are indicated in the figure.

The lifetime of the sdB on the extreme horizontal branch is of the same order as the one of the WD and we therefore derive a similar progenitor mass of more than 3 $M_\odot$, consistent with the disc kinematics and the constraints from binary formation scenarios.

9. Conclusions

Systems like CD-30°11223 are young, which is consistent with the non-detection of objects with such high RV-shifts in the course of the MUCHFUSS project so far (Geier et al. 2011, 2011). Most targets of this survey are faint subdwarfs located in the old halo population. The sdB-donor double-detonation channel is therefore predicted to occur in young stellar populations and to contribute to the SN Ia population with short delay time (Ruiter et al. 2009).

Given that systems like CD-30°11223 are progenitors of some thermonuclear SN, a rough estimate can be made of the rate of such events. The system CD-30°11223 is one out of ∼100 solved sdB binaries (Geier et al. 2011). About 50% of the known sdB stars are in close binary systems. So we can estimate the number fraction of systems like CD-30°11223 to be about 0.5% of the whole population of sdB stars. According to binary evolution calculations, the birthrate of such stars in our Galaxy is $\sim 5 \times 10^{-2}\,\mathrm{yr}^{-1}$ (Han et al. 2003). We therefore estimate the number of progenitor systems and the resulting SN Ia rate to be $\sim 2.5 \times 10^{-4}\,\mathrm{yr}^{-1}$. This is consistent with the theoretical birthrate predicted for the WD+He star channel ($\sim 3 \times 10^{-4}\,\mathrm{yr}^{-1}$, Wang et al. 2010), but more importantly, it is smaller than the SN Ia birthrate of $\sim 3 \times 10^{-3}\,\mathrm{yr}^{-1}$ and, therefore, consistent with observations (Capellaro & Turato 1997).

Although sub-Chandrasekhar scenarios in general have no well-defined explosion mass, the parameter space for the sdB binary progenitors turns out to be quite narrow. According to hydrodynamic simulations the minimum mass of the WD should be ∼0.8 $M_\odot$, because carbon burning is not triggered for objects of much lower mass (Sim et al. 2012). On the other hand, the WD must consist of carbon and oxygen to be able to explode as a SN Ia. This limits the mass to values lower than ∼1.1 $M_\odot$, because even more massive WDs consist of oxygen, neon, and magnesium and tend to collapse rather than explode. This mass range is further narrowed down by binary evolution calculations. Very close sdB+WD systems with companion masses around 0.8 $M_\odot$ are predicted to be formed in much higher numbers than binaries with more massive companions. Another important constraint is that the timespan from the binary formation after the CE to the SN Ia explosion must be shorter than the core helium-burning lifetime (∼100 Myr). Otherwise the sdB will turn into a WD before helium can be transferred. This restricts the orbital periods of possible sdB+WD progenitors to less than ∼0.07 d.

The double-detonation scenario with a hot subdwarf donor is the only proposed SN Ia scenario where both progenitors and remnants have been identified. Analysing a larger sample of these objects will allow us to put tight constraints on their properties and evolution.

Acknowledgements. Based on observations obtained at the European Southern Observatory, La Silla for programme 089.D-0265(A). Based on observations with the *William Herschel* Telescope (WHT) operated by the Isaac Newton Group at the Observatorio del Roque de los Muchachos of the Instituto de Astrofisica de Canarias on the island of La Palma, Spain. Based on observations made at the South African Astronomical Observatory (SAAO). Based on observations with the Southern Astrophysical Research (SOAR) telescope operated by the US National Optical Astronomy Observatory (NOAO), the Ministrio da Ciencia e Tecnologia of the Federal Republic of Brazil (MCT), the University of North Carolina at Chapel Hill (UNC), and Michigan State University (MSU). We acknowledge the Director of SOAR for making the time for these observations during Technical and Engineering nights on the telescope. A.I. acknowledges support from a research scholarship by the Elite Network of Bavaria. V.S. acknowledges funding by the Deutsches Zentrum für Luft- und Raumfahrt (grant 50 OR 1110) and by the Erika-Giehrl-Stiftung. S.G. and E.Z. are supported by the Deutsche Forschungsgemeinschaft (DFG) through grants HE1356/49-1 and HE1356/45-2, respectively. Finally, we want to thank the anonymous referee for helpful comments and suggestions.

References

Bloemen, S., Marsh, T. R., Østensen, R. H., et al. 2011, MNRAS, 410, 1787
Brown, W. R., Geller, M. J., Kenyon, S. J., & Kurtz M. J. 2005, ApJ, 622, L33
Capellaro, E., & Turatto, M. 1997, NATO ASI Series, 486, 77
Claret, A., & Bloemen, S. 2011, A&A, 529, 75
Copperwheat, C., Marsh, T. R., Dhillon, V. S., et al. 2010, MNRAS, 402, 1824
Edelmann, H., Napiwotzki, R., Heber, U., Christlieb, N., & Reimers, D. 2005, ApJ, 634, L181
Eggleton, P. P. 1971, MNRAS, 151, 351
Eggleton, P. P. 1972, MNRAS, 156, 361
Eggleton, P. P. 1973, MNRAS, 163, 279
Fink, M., Röpke, F. K., Hillebrandt, W., et al. 2010, A&A, 514, A53
Fontaine, G., Brassard, P., & Bergeron, P. 2001, PASP, 113, 409
Geier, S., Nesslinger, S., Heber, U., et al. 2007, A&A, 464, 299
Geier, S., Heber, U., Podsiadlowski, Ph., et al. 2010, A&A, 519, A25
Geier, S., Hirsch, H., Tillich, A., et al. 2011a, A&A, 530, A28
Geier, S., Maxted, P. F. L., Napiwotzki, R., et al. 2011b, A&A, 526, A39
Geier, S., Marsh, T. R., Dunlap, B. H., et al. 2013, ASP Conf. Ser., in press [arXiv:1209.4740]
Han, Z., Podsiadlowski, Ph., & Eggleton, P. P. 1994, MNRAS, 270, 121
Han, Z., Tout, C. A., & Eggleton, P. P. 2000, MNRAS, 319, 215
Han, Z., Podsiadlowski, Ph., Maxted, P. F. L., Marsh, T. R., & Ivanova, N. 2002, MNRAS, 336, 449
Han, Z., Podsiadlowski, Ph., Maxted, P. F. L., & Marsh, T. R. 2003, MNRAS, 341, 669
Heber, U., Reid, N., & Werner, K. 2000, MNRAS, 363, 198
Heber, U., Geier, S., Gänsicke, B. 2013, EPJ Web of Conferences, 43, 04002
Hirsch, H. A., Heber, U., O'Toole, S. J., & Bresolin, F. 2005, A&A, 444, L61
Irrgang, A., Wilcox, B., Tucker, E., & Schiefelbein, L. 2013, A&A, 549, A137
Justham, S., Wolf, C., Podsiadlowski, Ph., & Han, Z. 2009, A&A, 493, 1081
Kilic, M., Brown, W. R., Allende Prieto, C., et al. 2012, ApJ, 751, 141
Kovetz, A., Yaron, O., & Prialnik, D. 2009, MNRAS, 395, 1857
Kromer, M., Sim, S. A., Fink, M., et al. 2010, ApJ, 719, 1067
Landau, L. D., & Lifshitz, E. M. 1971, Classical theory of fields (Oxford: Pergamon Press)
Maxted, P. F. L., Marsh, T. R., & North, R. C. 2000, MNRAS, 317, L41
Maxted, P. F. L., Heber, U., Marsh, T. R., & North, R. C. 2001, MNRAS, 326, 1391

Napiwotzki, R., Karl, C. A., Lisker, T., et al. 2004a, Ap&SS, 291, 321
Napiwotzki, R., Yungelson, L., Nelemans, G., et al. 2004b, ASP Conf. Ser., 318, 402
Nelemans, G. 2009, Class. Quant. Grav., 26, 094030
Németh, P., Kawka, A., & Vennes, S. 2012, MNRAS, 427, 2180
Nomoto, K. 1982, ApJ, 257, 780
Pollacco, D. L., Skillen, I., Collier Cameron, A., et al. 2006, PASP, 118, 1407
Pols, O. R., Tout, C. A., Eggleton, P. P., & Han, Z. 1995, MNRAS, 274, 964
Pols, O. R., Schröder, K.-P., Hurley, J. R., Tout, C. A., & Eggleton, P. P. 1998, MNRAS, 298, 525
Roelofs, G. H. A., Groot, P. J., Benedict, G. F., et al. 2007, ApJ, 666, 1174
Roeser, S., Demleitner, M., & Schilbach, E. 2010, AJ, 139, 2440
Ruiter, A. J., Belczynski, K., & Fryer, C. 2009, ApJ, 699, 2026
Shakura, N., I., & Postnov, K. A. 1987, A&A, 183, L21
Sim, S., Röpke, F. K., Hillebrandt, W., et al. 2010, ApJ, 714, L52
Sim, S., Fink, M., Kromer, M., et al. 2012, MNRAS, 420, 3003
Vennes, S., Kawka, A., & Németh, P. 2011, MNRAS, 410, 2095
Vennes, S., Kawka, A., O'Toole, S. J., Németh, P., & Burton, D. 2012, ApJ, 759, L25
Verbunt, F., & Rappaport, S. 1988, ApJ, 332, 193
Wang, B., & Han, Z. 2009, A&A, 508, L27
Wang, B., & Han, Z. 2012, New Astron. Rev., 56, 122
Wang, B., Chen, X., Meng, X., & Han, Z. 2009a, ApJ, 701, 1540
Wang, B., Meng, X., Chen, X., & Han, Z. 2009b, MNRAS, 395, 847
Wang, B., Liu, Z., Han, Y., et al. 2010, Sci. China Ser. G, 53, 586
Winkler, F. P., Gupta, G., & Long, K. S. 2003, ApJ, 585, 324
Woosley, S. E., Taam, R. E., & Weaver, T. A. 1986, ApJ, 301, 601
Yoon, S.-C., & Langer, N. 2003, A&A, 412, 53